Available online at www.sciencedirect.com

ScienceDirect

Advances in Space Research 75 (2025) 2982–2993

ADVANCES IN SPACE RESEARCH (a COSPAR publication)

www.elsevier.com/locate/asr

Analytical estimation of probabilities of impact on Mars and Earth-Moon system for planetary protection assessment of Hayabusa2 extended mission ☆

Masahiro Fujita [1,*], Hajime Yano [2], Yuichi Tsuda [2]

3-1-1, Yoshinodai, Chuo-ku, Sagamihara, Kanagawa 252-5210, Japan

Received 26 December 2023; received in revised form 4 October 2024; accepted 10 November 2024
Available online 14 November 2024

Abstract

This paper reports the results of the estimation of the probabilities of impact on Mars, Earth, and the Moon for the asteroid probe Hayabusa2 in its extended mission. The probabilities of impact were estimated using an analytical method instead of a computationally expensive Monte Carlo simulation. The results show that the probability of impacting Mars is 5.45×10^{-7}, which is sufficiently small to meet the planetary protection requirements of the Committee on Space Research. The probabilities of impacting Earth and the Moon are also estimated as 0.0116 and 1.62×10^{-9}, respectively, which are found to be sufficiently small.

Keywords: Planetary protection; Asteroid sample return; Analytical method; Mars impact probability

1. Introduction

The asteroid probe Hayabusa2, developed by the Japan Aerospace Exploration Agency (JAXA) and launched in December 2014, completed its mission to the asteroid Ryugu and returned to Earth in December 2020, successfully delivering samples from Ryugu to Earth. Although the nominal mission ended with the return of the samples to Earth, an extended mission has been ongoing since then. The extended mission plans to explore two more asteroids, namely 2001 CC21 and 1998 KY26.

Planetary protection is essential for deep space exploration. When exploring celestial bodies, including the Moon, it is necessary to prevent their contamination by materials from Earth and, conversely, the contamination of Earth's environment by materials from these bodies, as stipulated in the United Nations Outer Space Treaty (United Nations, 1967). The Committee on Space Research (COSPAR) has developed international guidelines on planetary protection called the Planetary Protection Policy (PPP). According to these guidelines, space missions are classified into five categories based on factors such as their type and target body; countermeasures, such as analyses of the probability of impact and enumeration of the bioburden, for a given mission should be taken according to its category (COSPAR, 2021).

☆ Submitted to Advances in Space Research 16 December 2023.

* Corresponding author.
E-mail addresses: fujita.masahiro@ac.jaxa.jp, fujita.space336@gmail.com (M. Fujita), yano.hajime@jaxa.jp (H. Yano), tsuda.yuichi@jaxa.jp (Y. Tsuda).
[1] Graduate School of Engineering, Department of Aeronautics and Astronautics, The University of Tokyo, Japan.
[2] Institute of Space and Astronautical Science, Japan Aerospace Exploration Agency, Japan.

https://doi.org/10.1016/j.asr.2024.11.028

The Hayabusa2 nominal mission is classified as Category-II during its outbound journey (and thus needs to avoid impact with Mars under all mission scenarios) and Category-V during its inbound journey (corresponding to unrestricted Earth return). The COSPAR PPP does not place strict containment or quarantine provisions on the Hayabusa2 project. It does, however, require an analysis of the probability of impact of the spacecraft with Mars to be conducted under all possible mission scenarios. The probability must be less than 1×10^{-4} in the 50-year period after its launch (COSPAR, 2021). The estimation of Mars impact probability for the nominal mission was performed using the Monte Carlo method; the mission was approved by the COSPAR Planetary Protection Panel in 2012 (Chujo et al., 2016).

Since the production of the Hayabusa2 spacecraft was managed well below ISO 8 level conditions, it is classified as Category-III for the Mars impact conditions in the extended mission. The requirement is relaxed to 1×10^{-2} probability for 20 years and 5×10^{-2} between 20 and 50 years after launch. However, we impose a stricter condition for the following reason. Since Hayabusa2 landed on the C-type asteroid Ryugu, some portion of the spacecraft's surface has been contaminated by the material of Ryugu. Although the Ryugu surface and sub-surface materials were approved for the Category-V unrestricted Earth return by the COSPAR PPP, we applied the stricter condition of less than 1×10^{-4} for 50 years as the worst-case contamination level of the spacecraft (Category-II) to satisfy the Mars contamination level required by the COSPAR PPP.

The probability of impacting a celestial body can be estimated using either a numerical method or an analytical method. A typical numerical method is the Monte Carlo method, which randomly generates samples and propagates their trajectories. The Monte Carlo method has been utilized for various missions. For example, it was used for Juno's planetary protection analysis for Europa (Bernard et al., 2013). Monte Carlo simulation has also been applied to the estimation of the probability of impacting Mars in the Hayabusa2 nominal mission(Chujo et al., 2016).

Since the target body (e.g., Mars) in a planetary protection analysis is extremely small compared to the vastness of space, the Monte Carlo method requires a very large number of samples, resulting in a large computational cost. Analytical methods have a significantly lower computational cost (Wallace, 2015). In addition, trajectories with swing-by are very strongly divergent systems and behave chaotically. Therefore, it is almost impossible to evaluate them using Monte Carlo simulations. We propose a method to limit the scope of evaluation and to perform the covariance analysis to evaluate the probabilities analytically.

Although not required by the COSPAR PPP, it is important to estimate the impact probability of a spacecraft with Earth and the Moon from the viewpoints of science and risk to human life (see Section 4 for details).

This paper reports the results of the estimation of the probabilities of impact on Mars, Earth, and the Moon for the Hayabusa2 extended mission conducted using analytical methods that are computationally less expensive than the Monte Carlo method.

2. Mission and spacecraft design overview

Overviews of the nominal mission and the spacecraft design have been previously reported (Chujo et al., 2016). This section mainly focuses on the differences between the extended mission and the nominal mission.

2.1. Mission phases

The extended mission began immediately after the sample return to Earth in December 2020. The goals of the extended mission were planned based on engineering considerations, such as the relation between the remaining fuel and the orbital maneuvering required to reach the target object and the feasibility of the operation, and science considerations, such as the size, rotation speed, and type of the target object. The Earth-Asteroid-Earth-Earth-Asteroid scenario was selected (Hirabayashi et al., 2021). The milestones of the extended mission include:

1. Dec. 2020 Earth departure
2. Jul. 2026 2001 CC21 flyby
3. Dec. 2027 Earth swing-by 1
4. Jun. 2028 Earth swing-by 2
5. Jul. 2031 Rendezvous with 1998 KY26

Fig. 1. shows the planned trajectory of the Earth-Asteroid-Earth-Earth-Asteroid scenario, orbits of Earth and Venus, swing-by position, and flyby and rendezvous positions to the asteroids in the inertial coordinate system (J2000EC) and the Sun-Earth fixed coordinate system.

2.2. Spacecraft characteristics

An external view of Hayabusa2 is shown in Fig. 2. Hayabusa2 has four ion thrusters (μ10 engines) mounted on the $+X$ side of the body. The prelaunch xenon propellant payload was 66.5 kg (total ΔV of 3 km/s). Although the spacecraft is capable of simultaneously operating three of the four thrusters, one-thruster operation is to be exclusively applied in the extended mission. One thruster generates 10 mN of thrust at 2800 s of specific impulse.

The reaction control system (RCS) adopts a bipropellant, hydrazine/nitrogen tetroxide (NTO), system. Twelve 20-N thrusters are installed to realize six-degrees-of-freedom maneuverability. The RCS is used for trajectory correction maneuvers in the vicinity of third bodies in operations such as Earth swing-by, asteroid rendezvous, and flyby.

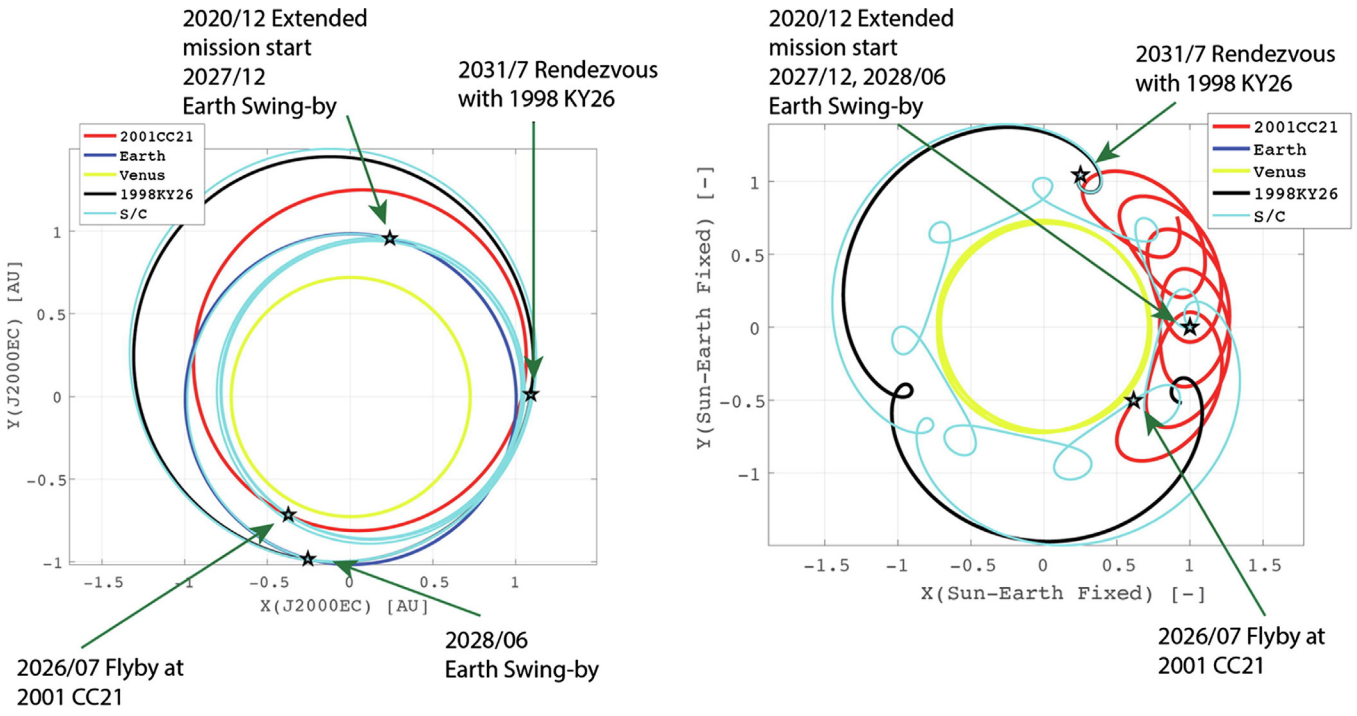

Fig. 1. Planned trajectory of Earth-Asteroid-Earth-Earth-Asteroid scenario (Hirabayashi et al., 2021).

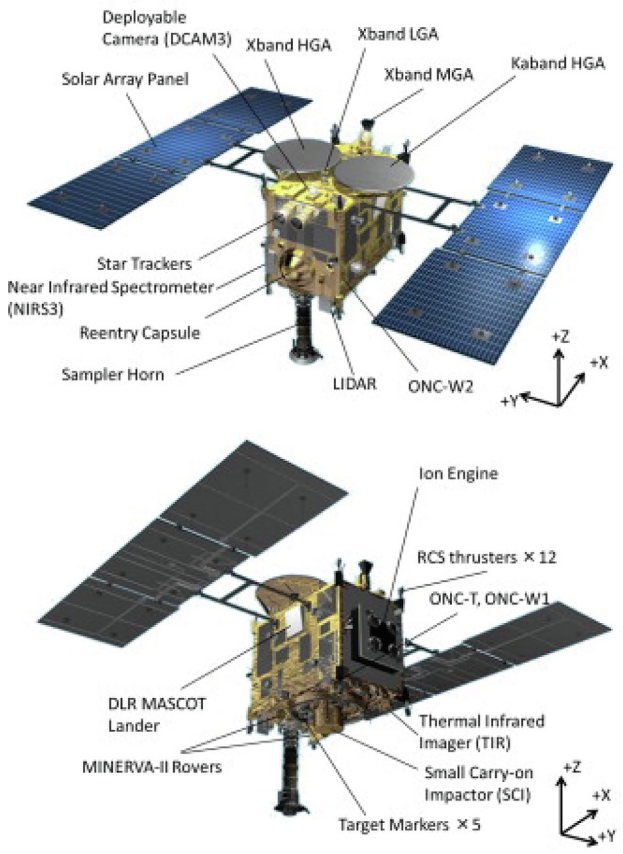

Fig. 2. External view of Hayabusa2 (Tsuda et al., 2013).

As of 2020 (at the Earth return), the amount of remaining ion engine system (IES) fuel was 32.5 kg (52.9% of the initial fuel mass) and the amount of remaining RCS fuel was 13.9 kg (29.2% of the initial fuel mass). See Tsuda et al. (2013) for details on the Hayabusa2 system design.

2.3. Spacecraft failure analysis

Possible failures of Hayabusa2 are assumed to have an internal (i.e., system failure) or external (i.e., meteoroid impact) cause. The estimation method used in this analysis for both types of cause is described below.

2.3.1. System failure rate

Hayabusa2 was designed and manufactured according to JAXA's system engineering and mission assurance standards. The IES is the most critical subsystem (other systems include data processing, communication, and power supply systems). Three of the four IES thrusters were designed to be operational for the 6-year nominal mission. The relation among the reliability R, failure rate λ, and time t can be expressed as

$$R = \exp(-\lambda t) \tag{1}$$

If $R = 0.75$ and $t = 6$ yr, the failure rate of the IES is $\lambda = 1.3 \times 10^{-4}$ per day. Thus, the reliability directly related to an impact, denoted by R_I , is expressed by

$$R_I(t) = 1 - (1 - R)^4 = 1 - \exp(-\lambda t) \tag{2}$$

Here, the failure rates of subsystems other than the IES are assumed to be sufficiently small compared to that of the IES and are thus ignored. The above method for estimating the system reliability (represented as Eq. (2) was applied to the analysis for the nominal mission (Chujo et al., 2016), and it is also applied to the analysis for the extended mission.

2.3.2. Meteoroid kill rate

The trajectory of the Hayabusa2 extended mission is between perihelion at 0.8 AU and aphelion at 1.4 AU. This mission will operate from 2020 to 2031 (Hirabayashi et al., 2021). During interplanetary cruising, hypervelocity impacts by meteoroids are inevitable. For the nominal mission from 2014 to 2020, Chujo et al. (2016) categorized three scenarios in which meteoroid impacts would fatally damage the spacecraft; these scenarios are also valid for the extended mission, as shown in Table 1. To derive the spacecraft kill rate, we assumed that the meteoroid flux was the average cumulative flux of meteoroids at a heliocentric distance of 0.8–1.4 AU. In the first scenario, all four IES grids are disrupted. The composite grid can be physically fractured by a hypervelocity impact by a meteoroid as small as 8×10^{-6} g. Since one of the four IES grids has a kill rate of 1.1×10^{-2} yr^{-1}, the kill rate for all four grids is 1.5×10^{-8} yr^{-1}. In the second scenario, one of the twelve RCS thrusters is penetrated, causing a malfunction or a fuel leakage. For this type of damage, the threshold meteoroid mass is estimated to be 10^{-4} g, which results in a kill rate of 1.3×10^{-4} yr^{-1}. In the third scenario, hypervelocity-impact-induced plasma is created on any of the external honeycomb panels of the spacecraft's main body, generating a dark current that may intrude into the interior circuit. For this type of damage, the threshold mass of the impacting meteoroid is estimated to be 10^{-3} g, which results in a kill rate of 1.7×10^{-2} yr^{-1}. For the extended mission, the third scenario has the highest kill rate. The total meteoroid impact kill rate is approximated as $\phi = 1.7 \times 10^{-2}$ yr^{-1}.

The meteoroid impact flux was calculated based on the meteoroid population model (Divine, 1993) updated by interplanetary mission results (Staubach et al., 2001), which varies by the heliocentric distance. We neglected minor contributions of sub-micron components such as interstellar dust and beta-meteoroids and assumed the isotropic distribution of interplanetary dust components at a given heliocentric distance. While these assumptions remain the same as our previous work (Chujo et al., 2016), one must note that the orbital parameters of the extended mission at 0.8–1.4 AU in 2020–2031 differ from those for its nominal mission at 0.96–1.42 AU in 2014–2020. The flux model predicts that the spacecraft would receive more meteoroid impacts as the spacecraft's trajectory gets closer to the Sun.

The total failure probability q in the period between t_i and t_j is calculated as

$$q(t_i, t_j) = R_I(t_i) - R_I(t_j) + \phi(t_j - t_i) \tag{3}$$

2.4. Navigation and guidance error

The policy for trajectory navigation and guidance for Hayabusa2 in the extended mission is basically the same as that in the nominal mission. Navigation and guidance are performed once a week based on range and range rate measurements. In the worst case, where the navigation process has problems, the orbit determination results are not updated for one month. In the nominal mission, the orbit determination error is 100 km (position, 1σ) and 1 m/s (velocity, 1σ) (Chujo et al., 2016), and it is same in the extended mission. In the guidance process, a new IES thrust plan is generated each week based on both the IES acceleration achieved during the previous week and the latest orbit determination results. In the nominal mission, the maximum guidance error for one month was calculated to 20 m/s (Chujo et al., 2016). Since only one of the four thrusters is operated in the extended mission, the maximum guidance error is estimated to be $20/3 = 6.67$ m/s.

3. Impact with Mars

There are two possible scenarios for impact with Mars: (i) direct impact with Mars without Earth swing-by and (ii) impact with Mars via Earth swing-by. In this section, we analytically estimate the probability of impact with Mars for the above two scenarios.

3.1. Direct impact with Mars without Earth swing-by

Before calculating the probability, we examine the possibility of impacting Mars from an energy point of view. Assuming a two-body problem in which only Sun's gravity is considered, Lambert's theorem is applied to calculate the

Table 1
Three scenarios of fatal damage to Hayabusa2 spacecraft by meteoroid impact during interplanetary cruising.

Scenario	1	2	3
Damage Case	Disruption of all of the four IES grids	Penetration of one of the 12 RCS thrusters	Impact-induced dark current intruding into the spacecraft interior circuit through the honeycomb external panels
Each Component Dimension	0.174 m^2 (per one IES)	0.041m^2 (per one RCS)	9.7m^2 (Total surface area of the spacecraft)
Threshold Meteoroid Mass	8×10^{-6} g	1×10^{-4} g	1×10^{-3} g
Averaged Cumulative Flux in the 2020–2031 trajectory	2×10^{-9}/m^2/s	10^{-10}/m^2/s	10^{-11}/m^2/s

minimum ΔV required to impact Mars within 50 years after launch (hereafter ΔV_{min}). In Lambert's theorem, the departure point is each point of the planned orbit in the extended mission, the flight time is the time from the failure time to the time within 50 years after launch, and the arrival point is set as each point of the Mars orbit divided into 360 equal points. ΔV_{min} is calculated for various values of these parameters.

Fig. 3 shows the relation between the failure date and ΔV_{min}. ΔV_{min} is a minimum (637 m/s) when failure occurs in August 2029; this value is much larger than the minimum guidance error of 6.67 m/s for the IES. Therefore, from an energy point of view, the probability of direct impact on Mars can be considered to be almost zero.

3.2. Impact on Mars via Earth swing-by

3.2.1. Energy-based estimates of probabilities of heading to Earth

The analysis in the previous section was performed for Earth; the results are shown in Fig. 4. In contrast to Fig. 3, the spacecraft reaches Earth with relatively small ΔV (i.e., energy). In particular, ΔV_{min} is very small after July 2026, when Hayabusa2 flies by the first asteroid (2001 CC21). The extended mission includes two Earth swing-bys, as noted in Section 2.1. Hayabusa2 will be injected into an orbit approaching Earth for the first Earth swing-by after July 2026. Therefore, after the first asteroid flyby, the energy required for the Earthward journey will be extremely low. If a failure occurs after July 2026, there is a possibility that the spacecraft will approach Earth, conduct Earth swing-bys, and accidentally transition to a Mars-bound trajectory. This possibility should be quantitatively investigated.

Due to the low energy required to reach Earth, it is possible for the spacecraft to accidentally make unscheduled Earth swing-bys at times other than the two nominal swing-bys and head toward Mars. If the probability of heading toward Mars by the second swing-by is P, then the probability of heading toward Earth by that swing-by can also be considered to be of the same order of magnitude $(O(P))$. The probability that the spacecraft will encounter Earth and swing-by again, and then head toward Mars can be estimated to be $O(P^2)$. Thus, if the probability of heading to Mars by the second Earth swing-by is sufficiently small, this scenario can be ignored. Fig. 5 shows this concept.

3.2.2. Overview of calculation algorithm for Mars impact

First, we search for the swing-by conditions required to reach Mars. Using Lambert's theorem, we find Earth departure velocities at the nominal swing-by required to reach Mars within 50 years after launch. We select the cases where the difference between the Earth departure velocity and the Earth arrival velocity just before the swing-by is less than a certain threshold value (3σ of the navigation and guidance deviation per month which is mentioned later) and then find the intersection points on the Earth B-plane that will allow the spacecraft to reach Mars. Here, the B-plane is defined to represent the motion of an object that conducts a swing-by in a coordinate system centered on the central celestial body. It is characterized by the relative velocity vector entering the sphere of influence. See Valsecchi et al. (2015) for details about the B-plane.

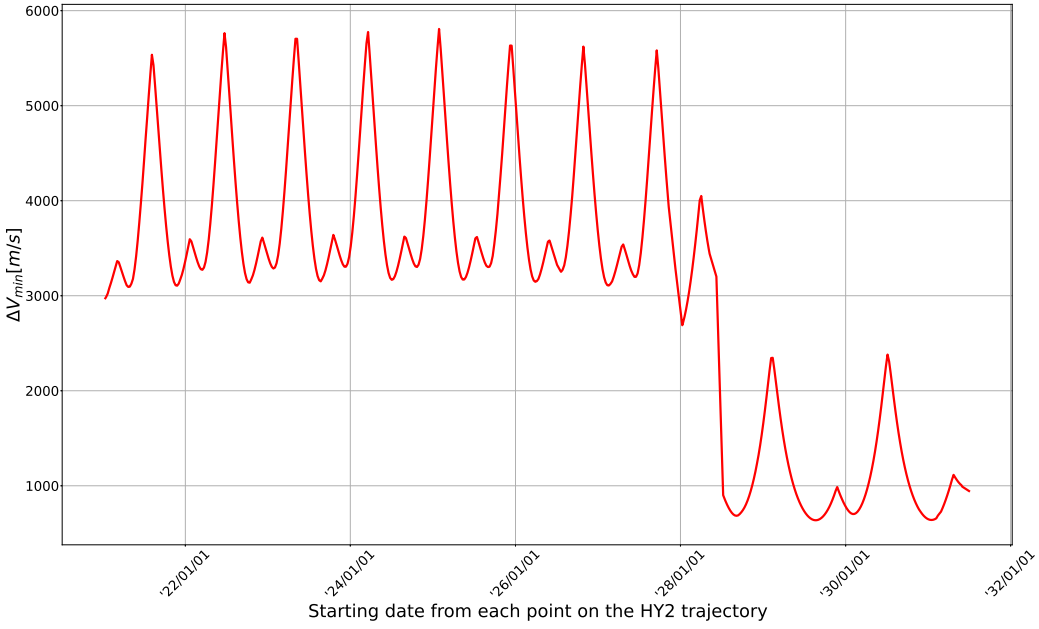

Fig. 3. ΔV_{min} required to reach Mars.

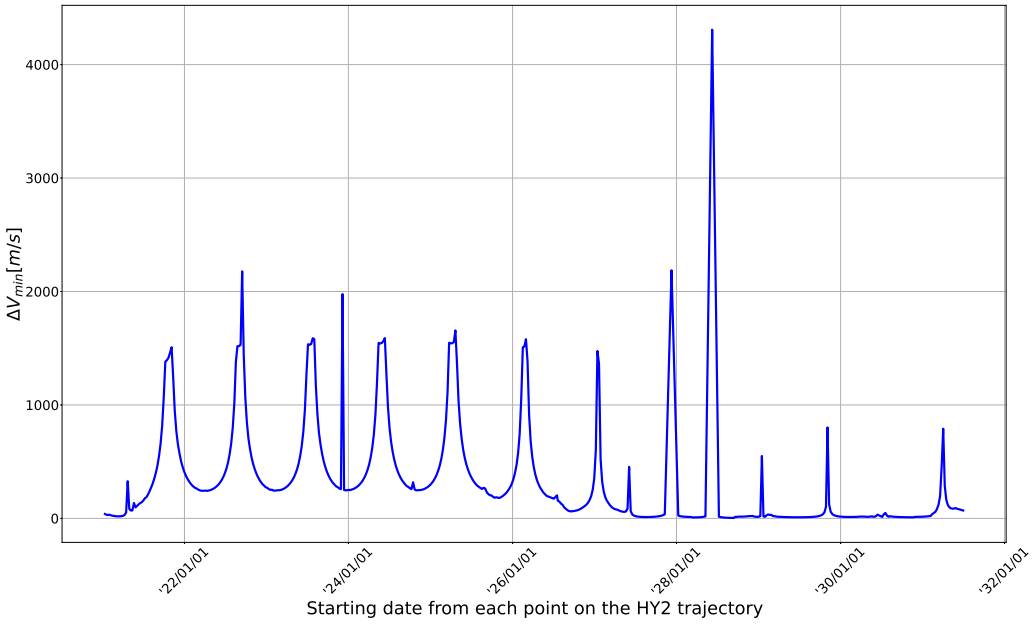

Fig. 4. ΔV_{min} required to reach Earth.

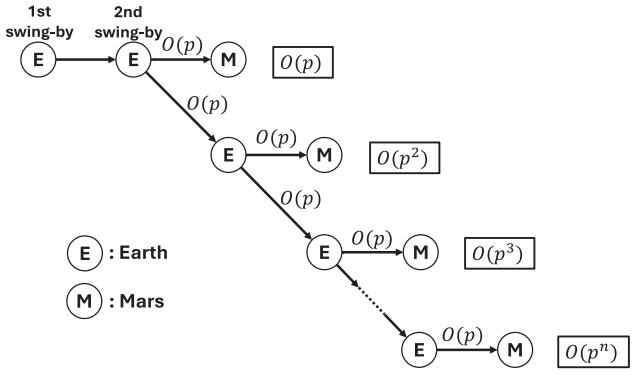

Fig. 5. Concept of the probability of Mars impact via Earth swing-bys.

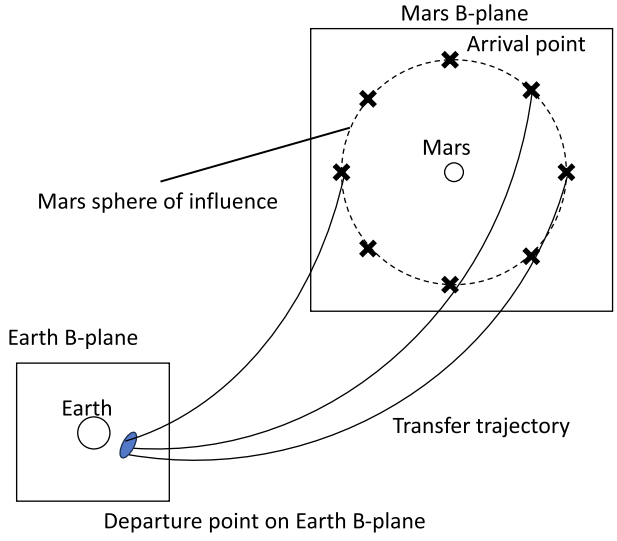

Fig. 6. Overview of departure point on Earth B-plane toward Mars.

Then, we calculate the probability of the spacecraft passing through each of these intersection points. For conservative estimation, we calculate the probability of entering the Mars sphere of influence (not the probability of impacting the main body of Mars). In each of the Mars arrival cases, the B-plane is defined based on the Mars arrival velocity. We solve Lambert's theorem using each point on the outer edge of the Mars sphere of influence on the Mars B-plane as an arrival point and obtain the departure points on the Earth B-plane. The outer edge of the Mars sphere of influence is represented as a closed curve on the Earth B-plane. Thus, a spacecraft that passes through the region enclosed by the closed curve will pass through the Mars sphere of influence. Fig. 6 shows an overview of this approach. Fig. 7 shows the intersection points that allow the spacecraft to reach the Mars sphere of influence on the Earth B-plane for the two Earth swing-bys. The blue stars are the points that allow the spacecraft to reach the center of Mars, obtained by Lambert's theorem, and the red points, which form closed curves around the blue stars, are the transit points that allow the spacecraft to reach the outer edge of the Mars sphere of influence. In other words, the area surrounded by the closed curves represents the transit region that allows the spacecraft to reach the Mars sphere of influence.

Monte Carlo simulations were performed to verify the validity of the analysis results. The results of the Monte Carlo simulation for the 10000 case are shown in Fig. 8. The figure shows the region near the transit region on Earth B-plane in Fig. 7a. The black dotted line indicates

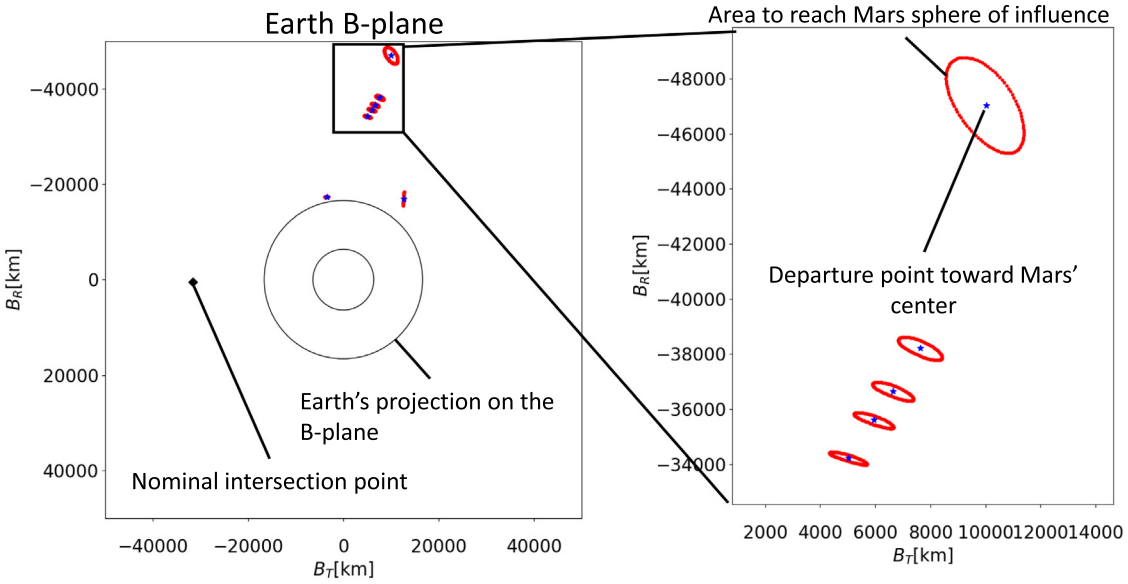

(a) Departure points at first swing-by timing.

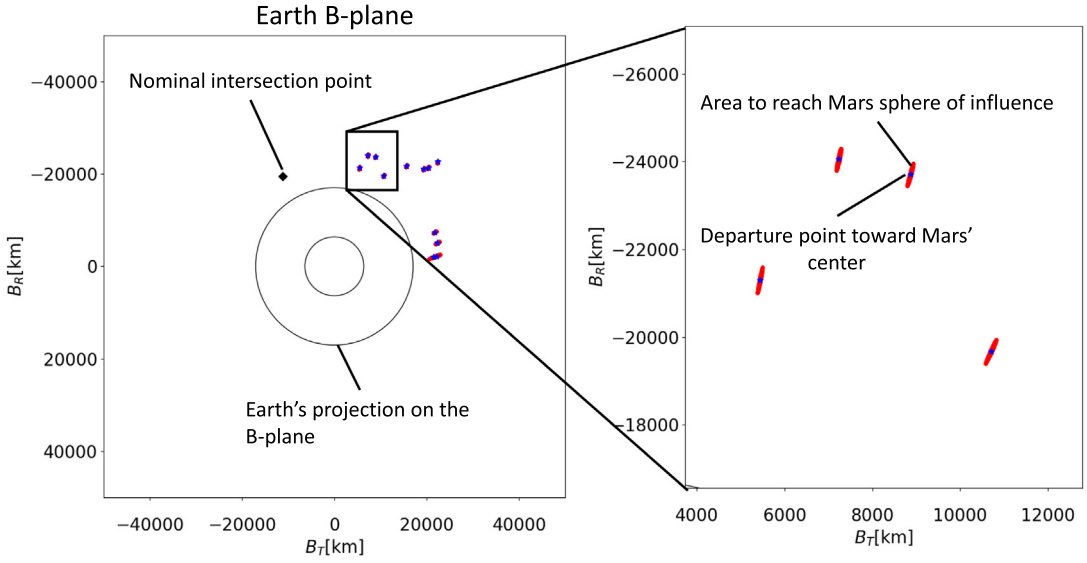

(b) Departure points at second swing-by timing.

Fig. 7. Departure points on Earth B-plane toward Mars.

the region through the edge of the sphere of influence obtained by the proposed method, and the blue dots indicate the transit region on the Earth-B plane for the Monte Carlo simulation of the transit through the Mars sphere of influence. In the Monte Carlo simulation, the 50-year interplanetary flight was calculated based on the real ephemeris. Both are in agreement, indicating that the proposed method is valid. The red points marked with asterisks in the figure correspond to the cases of orbits entering the sphere of influence that actually impact Mars. The figure clearly shows that there are very few cases in which orbits entering the sphere of influence actually collide with Mars. In other words, this method of analysis is conservative and valid enough to evaluate the possibility of impact by considering the probability of entering the sphere of influence.

Next, we calculate the probability of passing through the distribution shown in Fig. 7. Assuming that failure occurs at a certain time before the Earth swing-by, the error covariance matrix of the position and velocity of the spacecraft is propagated until the swing-by timing. The error ellipse for the position at the swing-by timing is plotted on the B-plane. The covariances at the failure timing are assumed based on the orbit determination accuracy and the IES guidance error. The deviation of the position is assumed to have a Gaussian distribution with standard deviation $\sigma = 100$ km based on the orbit

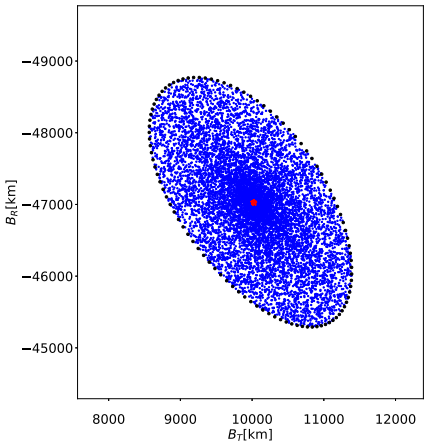

Fig. 8. Region on Earth B-plane entering Mars sphere of influence by Monte Carlo simulation.

determination accuracy. The deviation of the velocity is assumed to be $\sigma = \sqrt{1^2 + 6.67^2}$ m/s based on the orbit determination accuracy and the IES guidance error. Then, the error covariance matrix on the B-plane is computed using state transition matrices:

$$\Sigma_B = \Psi_B \Phi \Sigma_0 \Phi^T \Psi_B^T \tag{4}$$

where Σ_0 is the error covariance matrix in Cartesian coordinates at the failure time, Σ_B is the error covariance matrix on the B-plane at the swing-by time, Φ is the state transition matrix from the failure time to the swing-by time, and Ψ_B is the transformation matrix from Cartesian coordinates to the B-plane (Tapley et al., 2004). Since each transit region (i.e., the area surrounded by the closed curves) on the B-plane is sufficiently small compared to this error ellipse, the probability density can be considered to be uniform there. Multiplying the probability density by the area of the transit region toward Mars gives the probability p_j toward Mars if the failure occurred j steps earlier.

$$p_j \approx \sum_i^N f_j(\boldsymbol{x}_i) A_i \tag{5}$$

where A_i is the transit area (i.e., the area of the distribution in Fig. 7), $\boldsymbol{x}_i$ is the representative point of the transit region on the B-plane (the transit point toward the center of Mars), N is the number of transit regions, and f_j is the probability density function for the two-dimensional Gaussian distribution of the error ellipse on the B-plane when the spacecraft malfunctions j steps earlier.

$$f_j(\boldsymbol{x}) = \frac{1}{2\pi\sqrt{|\boldsymbol{P}_j|}} \exp\left(-\frac{1}{2}(\boldsymbol{x}-\mu_j)^T \boldsymbol{P}_j^{-1}(\boldsymbol{x}-\mu_j)\right) \tag{6}$$

where $\boldsymbol{\mu}_j$ represents the mean of the random variable vector and $\boldsymbol{P}_j$ the covariance matrix. To estimate A_i, the closed curve is approximated as an ellipse and its area is determined.

3.3. Probability of Mars impact

The Mars impact probability is calculated based on the spacecraft failure rate estimated in 2.3 using the calculation algorithm described in 3.2. The spacecraft impact probability P can be expressed by the following equation.

$$P = \int pqdt \tag{7}$$

where p is the Mars impact probability and q is the failure probability. Eq. (7) represents the time integration over the mission period considering the timing of a spacecraft malfunction. According to (Chujo et al., 2016), the integral can be discretized, which is fine enough to estimate the order of the probability. Eq. (7) can be discretized as follows:

$$P \approx \sum pq\Delta t \tag{8}$$

Δt is 1 week in this study.

Table 2 summarizes the probability of impact with Mars for the extended mission. The total probability of impact on Mars was estimated to be 5.45×10^{-7}, which satisfies the COSPAR requirement that the probability of impact on Mars within 50 years after launch must be less than 10^{-4}.

4. Impacts on Earth and Moon

In the previous section, we estimated the probability of a spacecraft impact with Mars. It is also important to estimate the collision probabilities for Earth and the Moon, which is expected to be the site of manned activities, including the Artemis mission.

In the extended mission, the energy required to reach Earth is relatively small, as shown in Fig. 4. In particular, after the flyby of the first asteroid, the orbit is adjusted for the Earth swing-bys, making the minimum ΔV required to head toward Earth extremely small. This may increase the probability of impact with Earth or the Moon.

In this section, we estimate the probabilities of impact with Earth and the Moon by applying the concept used to estimate the probability of impact with Mars (see previous sections).

4.1. Probability of entering Earth's sphere of influence

First, the probability of entering Earth's sphere of influence is estimated. A necessary condition for entry into the sphere of influence is that the spacecraft must pass through the Sun-Earth plane, as shown in Fig. 9. The spacecraft will enter the sphere of influence when the distance between the intersection point of the spacecraft's passage through the Sun-Earth plane and Earth is less than the radius of Earth's sphere of influence.

In the calculation of the probabilities, the error ellipse is propagated from the time of spacecraft failure to the time

Table 2
Probability of impact on Mars

Failure day	p	q	pq
2027/07/02	1.23e−14	2.22e−3	2.73e−17
2027/07/09	8.27e−13	2.60e−4	2.15e−16
2027/07/16	1.69e−10	5.20e−4	8.77e−14
2027/07/23	3.71e−9	5.20e−4	1.93e−12
2027/07/30	2.57e−8	5.19e−4	1.33e−11
2027/08/06	9.15e−8	5.19e−4	4.75e−11
2027/08/13	2.16e−7	5.19e−4	1.12e−10
2027/08/20	3.90e−7	5.18e−4	2.02e−10
2027/08/27	5.87e−7	5.18e−4	3.04e−10
2027/09/03	7.86e−7	5.17e−4	4.07e−10
2027/09/11	9.53e−7	5.17e−4	4.92e−10
2027/09/18	1.07e−6	5.16e−4	5.52e−10
2027/09/25	1.11e−6	5.16e−4	5.72e−10
2027/10/02	1.10e−6	5.15e−4	5.66e−10
2027/10/09	9.83e−7	5.15e−4	5.06e−10
2027/10/16	8.56e−7	5.14e−4	4.40e−10
2027/10/23	7.00e−7	5.14e−4	3.60e−10
2027/10/30	5.51e−7	5.14e−4	2.83e−10
2027/11/06	4.17e−7	5.13e−4	2.14e−10
2027/11/10	3.04e−7	5.13e−4	1.56e−10
2028/01/09	7.22e−7	2.27e−3	1.64e−9
2028/01/12	1.97e−6	2.53e−4	5.00e−10
2028/01/19	7.22e−6	5.06e−4	3.66e−9
2028/01/25	1.53e−5	5.06e−4	7.74e−9
2028/02/01	2.45e−5	5.06e−4	1.24e−8
2028/02/08	3.38e−5	5.05e−4	1.71e−8
2028/02/14	4.31e−5	5.05e−4	2.18e−8
2028/02/21	5.22e−5	5.04e−4	2.63e−8
2028/02/28	6.07e−5	5.04e−4	3.06e−8
2028/03/06	6.80e−5	5.04e−4	3.42e−8
2028/03/12	7.39e−5	5.03e−4	3.72e−8
2028/03/19	7.82e−5	5.03e−4	3.93e−8
2028/03/26	8.11e−5	5.02e−4	4.07e−8
2028/04/02	8.28e−5	5.02e−4	4.15e−8
2028/04/08	8.34e−5	5.02e−4	4.18e−8
2028/04/15	8.32e−5	5.01e−4	4.17e−8
2028/04/22	8.24e−5	5.01e−4	4.13e−8
2028/04/28	8.12e−5	5.00e−4	4.06e−8
2028/05/05	7.96e−5	5.00e−4	3.98e−8
2028/05/09	7.88e−5	2.50e−4	1.97e−8
Total			5.45e−7

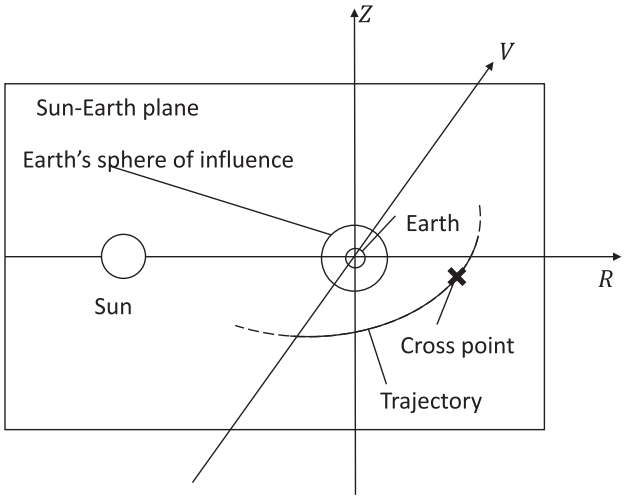

Fig. 9. Overview of cross point on Sun-Earth plane.

of the spacecraft's passage through the Sun-Earth plane. The probability of entering the sphere of influence is calculated from the positional relation between the error ellipse and the circle of Earth's sphere of influence, which is plotted on the Sun-Earth plane for the case of failure before the first swing-by and before the second swing-by in Fig. 10.

In the case of failure before the first swing-by, the error ellipse is very small compared to the sphere of influence, as shown in Fig. 10a. The intersection point included in the sphere of influence is the only point at the nominal swing-by timing; the other points of passage are far away from the sphere. For simplicity, the probability of entry to the sphere of influence is considered to be 1 when the intersection point is within the circle of the sphere (i.e., the intersection point at the timing of the nominal earth swing-by) and 0 when it is sufficiently far away from the sphere of influence.

In the case of failure before the second swing-by, an extremely large number of intersections are plotted in the sphere of influence, as shown in Fig. 10b. This is because after the first swing-by, the spacecraft enters a trajectory to meet Earth almost every half year for the second swing-by to be performed half a year later. A comparison of the orbital elements in Table 3 shows that orbital elements of the spacecraft are similar to those of Earth, indicating that the orbital period of the spacecraft is almost the same as that of Earth. Since the spacecraft makes the two nominal swing-bys at six-month intervals (Dec. 2027 and Jun. 2028), it will encounter Earth almost every 6 months.

In reality, once the spacecraft enters the sphere of influence, its trajectory will diverge significantly due to Earth's gravity. Therefore, the probability that it will re-enter Earth's sphere of influence after the swing-by is considered to be extremely low. In this probability estimation, only the probability at the first intersection (i.e., the timing of the nominal second swing-by) is estimated. Furthermore, as in the case of the failure before the second swing-by, the error ellipse is much smaller than Earth's sphere of influence, so the probability of entering the sphere of influence p can be considered to be 1.

The probability calculations are performed according to the above policy. There is a high probability of entry into the sphere of influence before the two Earth swing-bys. This is a natural consequence of the fact that the orbit is corrected by the IES in order to perform the swing-bys. Conversely, the possibility is negligible in periods other than before the two swing-bys. Therefore, only failures during the pre-swing-by period should be considered for calculating the probability of impact with Earth and the Moon. Considering the failure rate of the spacecraft q, the total probability of entering Earth's sphere of influence can be obtained as 0.0247 by calculating Eq. 8 with $p = 1$.

4.2. Probability of Earth impact

When estimating the probability of the spacecraft entering Earth's sphere of influence, it was sufficient to consider

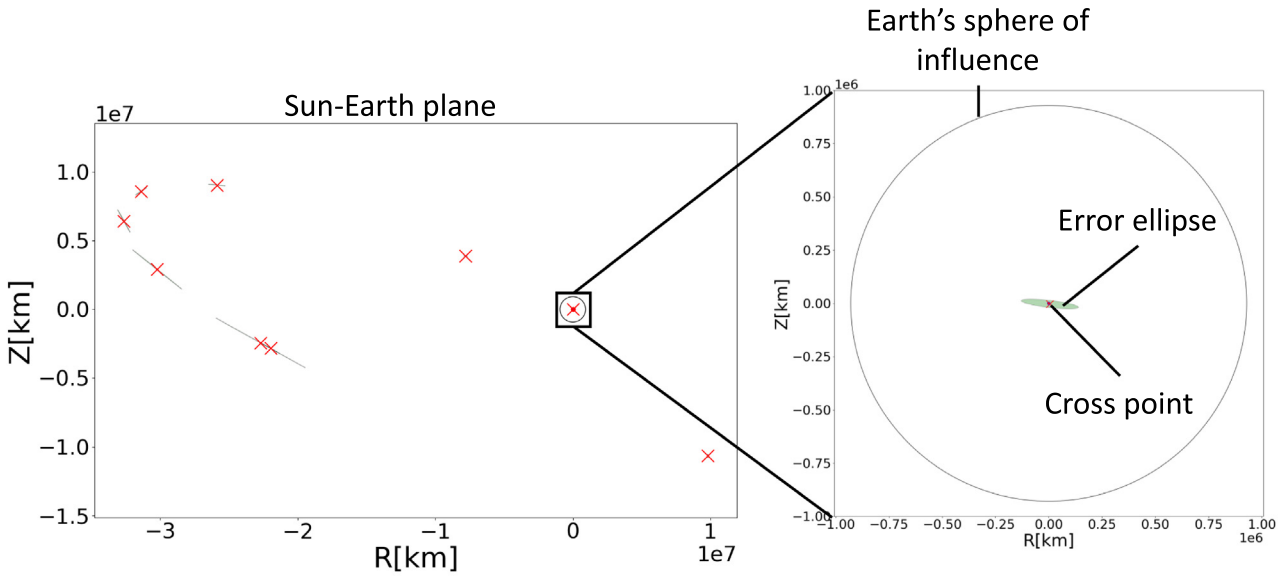

(a) Failure date: 2027/7/2 (before first nominal swing-by).

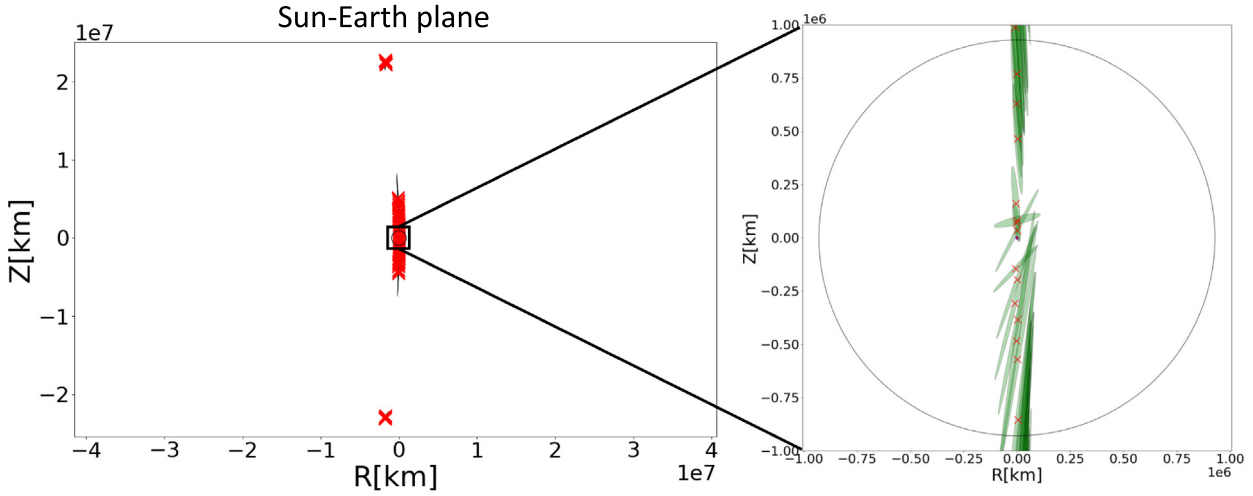

(b) Failure date: 2028/1/9 (before second nominal swing-by).

Fig. 10. Cross point and error ellipses on Sun-Earth plane.

Table 3
Orbital elements of Earth and the spacecraft.

	Semi-major axis a [km]	Eccentricity e	Inclination i [deg.]
Earth	1.497e8	0.0168	23.4
Spacecraft	1.496e8	0.0167	26.7

only Sun's gravity (i.e., the sun-centered two-body problem). However, when estimating the probability of impact with Earth, it is necessary to also consider the effect of Earth's gravity. In other words, we need to consider the problem not on the Sun-Earth plane but on the Earth B-plane. Among the intersections on the Sun-Earth plane obtained in the previous section, those included in Earth's sphere of influence are converted to the B parameters on the Earth B-plane. Earth and the position error of the spacecraft are projected onto the Earth B-plane, and the the positional relations between the two (the position error ellipse of the spacecraft and the projected circle of Earth) is used to determine the probability of collision with Earth. In other words, the collision probability is calculated from the probability density on the spacecraft position at Earth position and the area of the projected circle of Earth, which is very small compared to the error ellipse. If the area of the projected circle is A_i and the position of its center is x_i, the probability of impact on Earth p_j can be obtained using

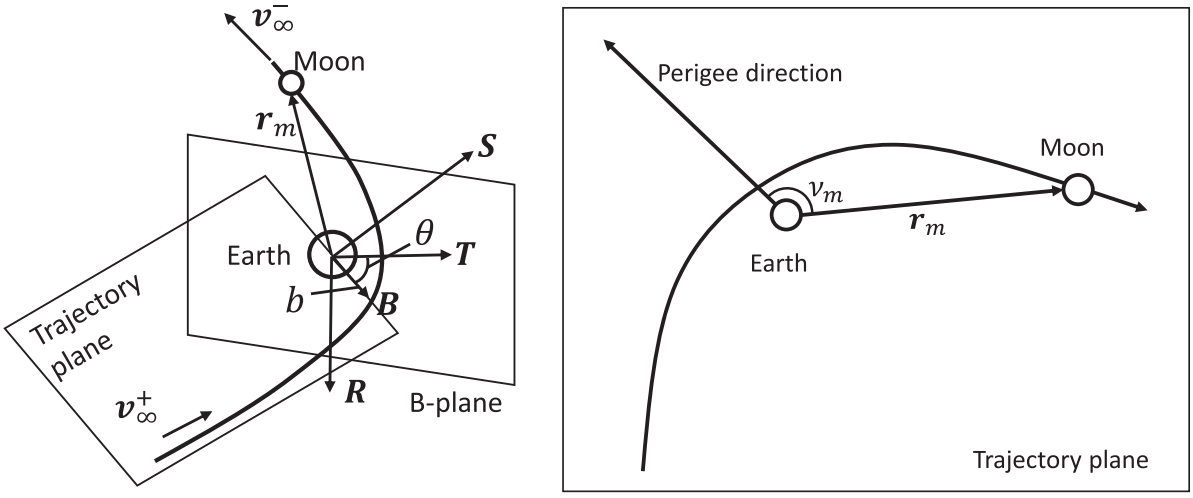

Fig. 11. Geometrical relations among parameters for Earth swing-by.

the same approach used to estimate the probability of impact on Mars in Eq. 5. Therefore, the probability of impact on the earth is estimated to be 0.0116 by Eq. 8.

4.3. Probability of Moon impact

The scenarios of impact with the Moon can be considered to be a direct impact with the Moon after Hayabusa2 enters Earth's sphere of influence and an impact with the Moon after an Earth swing-by. The positional relation between the spacecraft's transit area and the lunar orbit before and after the two nominal Earth swing-bys should be taken into account. In the case of direct impact with the Moon, the lunar orbit is projected onto Earth's B-plane and the positional relation between this orbit and the error ellipse related to the position of Hayabusa2 is considered. On the other hand, in the case of an impact with the Moon after an Earth swing-by, we consider the positional relationship between the spacecraft's error ellipse and a transit point on Earth's B-plane that satisfies such a condition.

Fig. 12a shows the maximum positional error ellipse and the lunar orbit at the time of the first nominal swing-by on the B-plane. The lunar orbit is sufficiently larger than the error ellipse, so the possibility of a direct impact with the Moon is negligible. In addition, there is no transit region on the B-plane toward the Moon after the Earth swing-by, and thus the probability of impact is negligible. Therefore, the probability of impact with the Moon due to the spacecraft's failure before the first Earth swing-by is negligible.

Fig. 12b shows the maximum positional error ellipse and the lunar orbit at the time of the second Earth swing-by. The lunar orbit is sufficiently large compared to the error ellipse, so the possibility of a direct impact with the Moon is negligible. On the other hand, the green dots in the figure indicate a region where the spacecraft heads toward the Moon after the swing-by. Since this region is within the error ellipse, it is necessary to quantitatively estimate this probability. For this purpose, it is necessary to determine the area of this transit region.

The expansion rate of the position error from the Earth swing-by timing to the timing of the passage of the Moon is obtained to determine the area of the transit region. The area of the Moon itself is projected onto the Earth B-plane using the expansion rate. Fig. 11 shows the geometrical relations. The position vector of the spacecraft at the Moon's position $\boldsymbol{r_m}$ is expressed as follows using the vector $\boldsymbol{S}, \boldsymbol{T}, \boldsymbol{R}$ to define the Earth B-plane:

$$\boldsymbol{r_m} = r_m\left(\boldsymbol{S}\sin\nu_m + \frac{\boldsymbol{B}}{b}\cos\nu_m\right) \tag{9}$$

$$\frac{\boldsymbol{B}}{b} = \begin{bmatrix} T_x\cos\theta + R_x\sin\theta \\ T_y\cos\theta - R_y\sin\theta \\ R_z\sin\theta \end{bmatrix} \tag{10}$$

where $\boldsymbol{S}$ is parallel to the hyperbolic excess velocity at the entry into the sphere of influence. $\boldsymbol{T}$ is the axis orthogonal to $\boldsymbol{S}$ on the B-plane and parallel to the ecliptic plane. $\boldsymbol{R}$ is defined as $\boldsymbol{R} \equiv \boldsymbol{S} \times \boldsymbol{T}$. The indices x, y, z refer to the element in the inertial coordinate system. $\boldsymbol{B}$ is the so-called impact parameter, $b = |\boldsymbol{B}|$, and θ is the angle between $\boldsymbol{B}$ and $\boldsymbol{T}$. ν_m is the true anomaly of the Moon's position.

From the above equations, the amount of change in $\boldsymbol{r_m}$ when b and θ change slightly is obtained. In other words, the following Jacobian matrix J can be obtained.

$$\delta\boldsymbol{r_m} = J\begin{bmatrix}\delta b \\ \delta\theta\end{bmatrix} \tag{11}$$

where δ represents change. When $\delta\boldsymbol{r_m} = \begin{bmatrix} R_m & R_m & R_m \end{bmatrix}^T$, the area of the transit region is determined to be 2196.6 [km^2], where R_m is the radius of the Moon ($R_m = 3,474.8$ [km]). Since the transit region is sufficiently smaller than

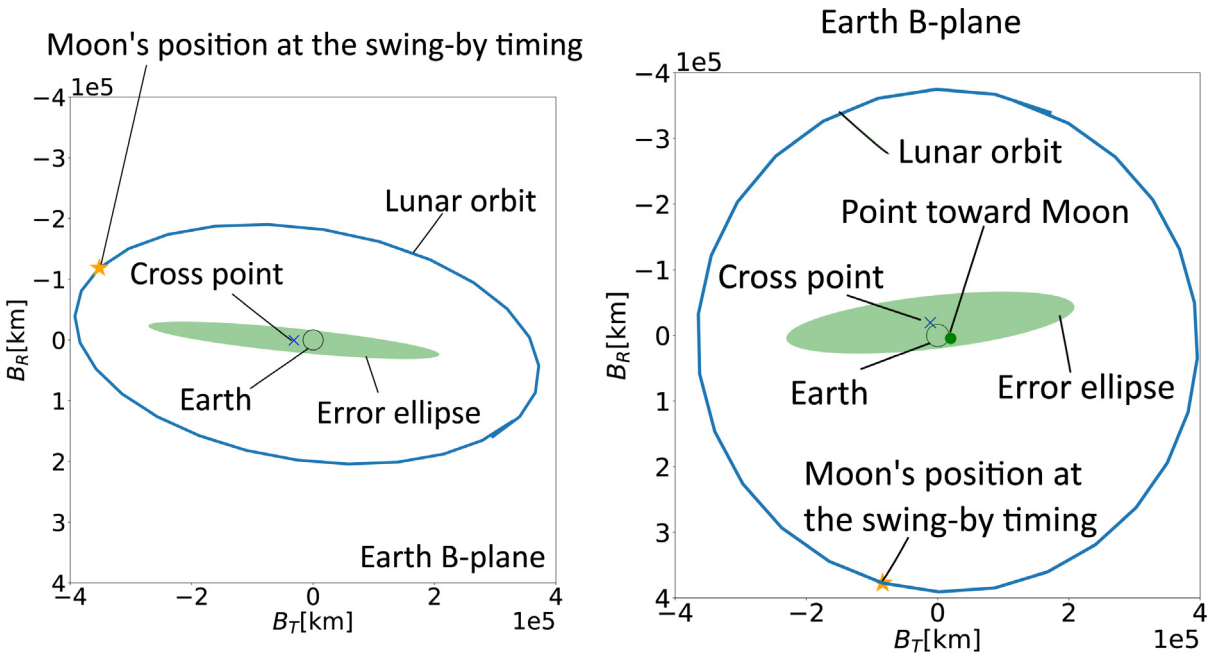

(a) Failure date: 2027/7/2 (before first nominal swing-by).

(b) Failure date: 2028/1/9 (before second nominal swing-by).

Fig. 12. The error ellipse and the lunar orbit projected on the Earth B-plane.

the error ellipse, the total probability of impact with the Moon is calculated as 1.62×10^{-9} using the method mentinoed in 3.3.

Although there is no clear standard for the probability of impact with the Moon, the obtained value is sufficiently small compared to the probability of impact with Mars required by COSPAR.

5. Conclusion

In this paper, an analytical method that included a covariance analysis was used to quantitatively estimate the probability of impact with Mars, Earth, and the Moon for the extended mission of the asteroid probe Hayabusa2. It was found that the Mars impact probability is extremely small (5.45×10^{-7}) and thus satisfies the planetary protection requirements set by COSPAR. The impact probabilities for the Moon were also found to be 0.0116 and 1.62×10^{-9}, respectively.

Declaration of Competing Interest

The authors declare that they have no known competing financial interests or personal relationships that could have appeared to influence the work reported in this paper.

References

Bernard, D.E., Abelson, R.D., Johannesen, J.R., et al., 2013. Europa planetary protection for juno jupiter orbiter. Adv. Space Res. 52 (3), 547–568. https://doi.org/10.1016/j.asr.2013.03.015.

Chujo, T., Tsuda, Y., Shimizu, Y., et al., 2016. Mars impact probability analysis for the hayabusa-2 neo sample return mission. Adv. Space Res. 57 (9), 1991–2002. https://doi.org/10.1016/j.asr.2015.07.042.

COSPAR, 2021. Policy on planetary protection.

Divine, N., 1993. Five populations of interplanetary meteoroids. J. Geophys. Res.: Planets 98 (E9), 17029–17048.

Hirabayashi, M., Mimasu, Y., Sakatani, N., et al., 2021. Hayabusa2 extended mission: New voyage to rendezvous with a small asteroid rotating with a short period. Adv. Space Res. 68 (3), 1533–1555, URL.

Staubach, P., Grün, E., Matney, M.J., 2001. Synthesis of observations. In: Interplanetary Dust. Springer, pp. 347–384.

Tapley, B.D., Schutz, B.E., H., G., 2004. Statistical orbit determination. Elsevier.

Tsuda, Y., Yoshikawa, M., Abe, M., et al., 2013. System design of the hayabusa 2—asteroid sample return mission to 1999 ju3. Acta Astronaut. 91, 356–362. https://doi.org/10.1016/j.actaastro.2013.06.028.

United Nations, 1967. Treaty on principles governing the activities of states in the exploration and use of outer space, including the moon and other celestial bodies.

Valsecchi, G., Alessi, E., Rossi, A., 2015. An analytical solution for the swing-by problem, volume 123. Springer.

Wallace, M.S., 2015. A massively parallel bayesian approach to planetary protection trajectory analysis and design. In AAS/AIAA Astrodynamics Specialist Conference, Vail, Colorado.